Materials Science and Engineering A 442 (2006) 292-296.

Hydrogen induced structural relaxation in bulk metallic glasses

K. Yamagishi, H. Tanimoto, H. Mizubayashi*
Institute of Materials Science, University of Tsukuba, Tsukuba 305-8573, Japan

Abstract

In order to clarify the hydrogen induced structural relaxation (HISR) of hydrogenated bulk and marginal metallic glasses (BMG and MMG), the hydrogen concentration (C_H) dependence of the peak temperature (T_p) and the peak height (Q^{-1}_p) of the hydrogen internal friction peak (HIFP) in *a*-$Zr_{55}Cu_{30}Al_{10}Ni_5$ (numbers indicate at.%) (BMG), *a*-$Zr_{54}Cu_{30}Al_{10}Ni_5Si_1$ (MMG) and *a*-$Zr_{40}Cu_{49}Al_{10}Si_1$ (MMG) were studied. It is found that the T_p *vs.* C_H data and the Q^{-1}_p *vs.* C_H data are well explained by the relationships of $T_p = \Delta T_p \exp(-C_H/\tau_H) + T_{p,0}$ and $Q^{-1}_p \propto \ln(C_H/\tau_H)$, respectively, not only for all the present metallic glasses but also for various Zr-base BMG and MMG reported. The characteristic C_H dependence of T_p and Q^{-1}_p was attributed to effects of the HISR. The detailed features of the C_H dependence of T_p and Q^{-1}_p were discussed in the light of material parameters and HISR.

Keywords: Metallic glass; Hydrogen; Internal friction; Structural relaxation
*Corresponding author. Fax: +81-29-853-4490. E-mail: mizubayashi@ims.tsukuba.ac.jp

1. Introduction

A recent feasibility study of hydrogenated Zr-base metallic glasses as the high-damping and high-strength materials [1-3] has evoked the internal friction works on hydrogenated bulk metallic glasses [4-9]. In these materials, the peak height, Q^{-1}_p, and the peak temperature, T_p, of the hydrogen induced internal friction peak (HIFP) and the tensile strength are indicative of the high-damping and high-strength performance. Although hydrogenated metallic glasses are very brittle after heavy hydrogenation, the tensile strength of metallic glasses tend to increase with increasing hydrogen concentration below a few tens percent [1-3]. It is known that T_p shows a decrease with increasing hydrogen concentration (C_H) for various metallic glasses [10]. Such a decrease in T_p has been explained by a change in the chemical potential of hydrogen in metallic glasses with increasing C_H [11,12]. On the other hand, recent intensive study on the HIFP for low C_H for various metallic glasses revealed that the decrease in T_p observed for low C_H was much stronger than that expected from the chemical potential of hydrogen [1-10], indicating that the hydrogen induced structural relaxation (HISR) [13] may play an important role. In the present work, the hydrogen concentration dependence of T_p and Q^{-1}_p for low C_H were studied in the light of HISR. Specimens prepared here were amorphous (*a*) $Zr_{55}Cu_{30}Al_{10}Ni_5$ (numbers indicate at.%) as an example of bulk metallic glasses (BMG)

[14] and *a*-$Zr_{54}Cu_{30}Al_{10}Ni_5Si_1$ as a silicon-modified BMG. As a reference material, *a*-$Zr_{40}Cu_{49}Al_{10}Si_1$ was revisited as a silicon-modified marginal metallic glass (MMG) which showed the highest T_p in the as hydrogen charged state among various a-alloys [2]. The present results will be discussed together with the previous data.

2. Experimental

Alloy ingots were prepared by arc-melting. Amorphous ribbon specimens of *a*-$Zr_{55}Cu_{30}Al_{10}Ni_5$, *a*-$Zr_{54}Cu_{30}Al_{10}Ni_5Si_1$ and *a*-$Zr_{40}Cu_{49}Al_{10}Si_1$ were prepared by melt spinning in a high-purity Ar gas atmosphere, where the thickness and the width of ribbons were about 30 μm and 1 mm, respectively. The specimen surfaces were polished mechanically in water avoiding heating up during polishing to remove a surface layer and to smoothen. Hydrogen charging was made electrolytically in 0.1N H_2SO_4 solution at room temperature (RT). The hydrogen charged specimen was aged for a few days at RT before measurements to homogenize the hydrogen distribution in the specimen. Specimen *a*-$Zr_{40}Cu_{49}Al_{10}Si_1$ was annealed at 400 K in order to complete the probable thermal structural relaxation prior to the measurements of internal friction, of length change and of X-ray diffraction (XRD). The internal friction, Q^{-1}, and the resonant frequency, f, were measured by means of the vibrating reed method at about 300 Hz and the strain amplitude of 10^{-6}. The internal friction measurements were conducted in the temperature range between 80 K and 360 K. A change in the specimen length, $\Delta L/L$, due to the hydrogenation was measured by an optical microscope with a micrometer stage. The XRD measurements were made by the conventional θ-2θ scan using the Cu Kα radiation. The hydrogen concentration, C_H, was determined by the thermal desorption method similar to that mentioned in [13].

3. Results

Figures 1(a) and 1(b) show examples of HIFPs observed at ~300 Hz in *a*-$Zr_{55}Cu_{30}Al_{10}Ni_5$ and *a*-$Zr_{54}Cu_{30}Al_{10}Ni_5Si_1$ specimens with various C_H, respectively The HIFP was observed as a very broad peak accompanied with the low temperature tail, indicating that the activation energy shows a wide distribution as already reported but for *a*-CuTi [15]. As seen in Figs. 1(a) and 1(b) for both the *a*-$Zr_{55}Cu_{30}Al_{10}Ni_5$ and *a*-$Zr_{54}Cu_{30}Al_{10}Ni_5Si_1$ specimens: T_p of HIFP shows a rapid decrease with increasing C_H below about 15 at% and then tends to show saturation for higher values: $Q^{-1}{}_p$ also tends to show saturation following a rapid increase with increasing C_H.

Figure 2(a) shows the T_p *vs*. C_H data observed for the reference material (MMG) *a*-$Zr_{40}Cu_{49}Al_{10}Si_1$ (after 400 K annealing) and the bulk metallic glass (BMG) *a*-$Zr_{55}Cu_{30}Al_{10}Ni_5$ together with those reported for (BMG) *a*-$Zr_{60}Cu_{30}Al_{10}$ [1]. It was found for various a-alloys that the T_p *vs*. C_H data can be well explained by,

$$T_p = \Delta T_p \exp(-C_H/\tau_H) + T_{p,0}\,, \qquad (1)$$

where ΔT_p and τ_H have usual meanings and $T_{p,0}$ is the ultimate value of T_p found at the high C_H region. As will be mentioned, ΔT_p is indicative of the distance of the glass structure measured from the ultimate glass after the HISR. Figures 2(b) and 2(c) are enlarged redrawing of the T_p *vs*. C_H data of fig. 2(a), but here the $\ln(T_p\text{-}T_{p,0})$ is plotted against C_H together with the results obtained in the silicon-modified (BMG) *a*-$Zr_{54}Cu_{30}Al_{10}Ni_5Si_1$ and in other metallic glasses previously investigated [2]. It is more clearly seen in Figs. 2(b) and 2(c)

that the T_p *vs.* C_H data observed for various metallic glasses are well explained by Eq. (1). Figure 3 shows the ΔT_p *vs.* τ_H data found for various Zr-Cu base metallic glasses, *a*-$Zr_{50}Ni_{50}$ and *a*-$Cu_{50}Ti_{50}$ [1-3,13,15]. In Fig. 3, the ΔT_p *vs.* τ_H data found for all the Zr-Cu base metallic glasses and *a*-$Zr_{50}Ni_{50}$ and *a*-$Cu_{50}Ti_{50}$ fall around the dashed line 1 (Group 1) except the data found for *a*-$Zr_{55}Cu_{30}Al_{10}Ni_5$, *a*-$Zr_{54}Cu_{30}Al_{10}Ni_5Si_1$ and *a*-$Zr_{50}Cu_{50}$ classified as Group 2. In this Fig. 3, *a*-$Zr_{40}Cu_{49}Al_{10}Si_1$ shows the highest T_p in the as charged state among various Zr-Cu base metallic glasses [2]: after 400 K annealing, ΔT_p markedly decreases and fits well the dashed line 1. This finding denotes that the strong thermal structural relaxation in the as charged state took place in *a*-$Zr_{40}Cu_{49}Al_{10}Si_1$. It is noted that BMGs *a*-$Zr_{60}Cu_{30}Al_{10}$ and *a*-$Zr_{55}Cu_{30}Al_{10}Ni_5$ are classified as the Group 1 and the Group 2, respectively, and Zr-Cu base metallic glasses found in the Group 2 are those with the compositional Zr concentration between 50 at% and 55 at%.

Figure 4 (a) shows the Q^{-1}_p *vs.* C_H data observed for *a*-$Zr_{55}Cu_{30}Al_{10}Ni_5$ and *a*-$Zr_{54}Cu_{30}Al_{10}Ni_5Si_1$, where Q^{-1}_p increased monotonously showing the tendency of saturation. Figure 4(c) is redrawing of Fig. 4(a) but here Q^{-1}_p is plotted against $\ln(C_H/\tau_H)$. Figure 4(b) shows the relaxation strength, S_t, *vs.* $\ln(C_H/\tau_H)$ data, where S_t was evaluated as the modulus defect observed in the *f* data between 80 K and 360 K. In Fig. 4(b), S_t shows a linear increase with increasing $\ln(C_H/\tau_H)$ in the whole range. The Q^{-1}_p *vs.* $\ln(C_H/\tau_H)$ data shown in Fig. 4(c) is very similar to those for S_t except for $\ln(C_H/\tau_H)$ below -1 or C_H below 5.5 at%. It is noted that Q^{-1}_p and S_t measure the constituent relaxation strength at around T_p and the total relaxation strength including the low temperature tail of the HIFP, respectively. Figures 5(a) and (b) are similar to Fig. 4(c) but display the data of : *a*-$Zr_{40}Cu_{50}Al_{10}$; *a*-$Zr_{40}Cu_{49}Al_{10}Si_1$ in the as charged state ; *a*-$Zr_{40}Cu_{49}Al_{10}Si_1$ after 400 K annealing ; *a*-$Zr_{60}Cu_{30}Al_{10}$ and *a*-$Zr_{59}Cu_{30}Al_{10}Si_1$. The linear increase in Q^{-1}_p with increasing $\ln(C_H/\tau_H)$ can be commonly seen except that the deviatory high Q^{-1}_p data were observed in the as charged state for *a*-$Zr_{40}Cu_{49}Al_{10}Si_1$ here and *a*-$Zr_{40}Cu_{50}Al_{10}$ [2] and *a*-$Zr_{60}Cu_{30}Al_{10}$ [1].

Figure 6 shows changes in the specimen length, $\Delta L/L_0$, due to hydrogenation observed for a-$Zr_{40}Cu_{49}Al_{10}Si_1$ in the as charged state and those measured after 400 K annealing, where $\Delta L/L_0$ showed the almost linear increase with increasing C_H. The hydrogen induced volume expansion, $(\Delta V/V)_H$ ($\approx 3(\Delta L/L_0)$), per unit C_H seen in Fig. 6 is very similar to that reported for various metallic glasses [16,17]. The $\Delta L/L_0$ data shown in Fig. 6 indicate that $(\Delta V/V)_H$ remained unchanged after 400 K annealing in the present experimental accuracy.

4. Discussion

As already mentioned, the decrease in T_p due to a change in the chemical potential of hydrogen in metallic glasses with increasing C_H [11,12] is expected to be a function of the constituent concentration of alloy elements with hydrogen affinity. On the other hand, as it can be evaluated from the slopes (Eq. 1) of the plots of Figs. 2(b) and 2(c), τ_H ~14 at.% found in *a*-$Zr_{40}Cu_{50}Al_{10}$ or *a*-$Zr_{40}Cu_{49}Al_{10}Si_1$ is much larger than τ_H ~5 at.% found in *a*-$Zr_{60}Cu_{30}Al_{10}$, indicating that the decrease in T_p with increasing C_H is mainly associated with the HISR. Then the ΔT_p *vs.* τ_H data shown in Fig. 3 may be indicative of the HISR in various metallic glasses. As seen in Fig. 2 or estimated from the data reported in Refs. [1-7,9,10], $T_{p,0}$ in Zr-base metallic glasses is found near 200 K, which is T_p of the HIFP in both Zr-base BMGs and MMGs after completion of the HISR, the ultimate glass after the HISR hereafter. In other words, ΔT_p is indicative of the distance of the glass structure measured from the ultimate glass after the HISR, where an increase in the HISR is expected with increasing ΔT_p as observed for *a*-$Zr_{40}Cu_{49}Al_{10}Si_1$. For the Group 1 metallic glasses shown in Fig. 3, τ_H increases with

increasing ΔT_p, where ΔT_p and τ_H are the lowest for *a*-$Zr_{60}Cu_{30}Al_{10}$ (BMG) and *a*-$Cu_{50}Ti_{50}$ (MMG) among those for the Group 1 metallic glasses. On the other hand, the crystallization volume, $(\Delta V/V)_x$, is 0.3 % for *a*-$Zr_{60}Cu_{30}Al_{10}$ [18] and 0.8 % for *a*-$Cu_{50}Ti_{50}$ [19], respectively. For the Group 2 metallic glasses shown in Fig. 3, $(\Delta V/V)_x$, is 0.4 % for *a*-$Zr_{55}Cu_{30}Al_{10}Ni_5$ [18] and 2.1 % for *a*-$Zr_{50}Cu_{50}$ [20], respectively. This is indicative that the correlation between $(\Delta V/V)_x$ and ΔT_p and/or τ_H is weak. No changes in $\Delta L/L_0$ observed for the thermal structural relaxation of *a*-$Zr_{40}Cu_{49}Al_{10}Si_1$ shown in Fig. 6 suggest that the structural relaxation responsible for changes in T_p is hardly associated with a change in the specimen volume. The linear relationship found between $Q^{-1}{}_p$ and $\ln(C_H/\tau_H)$ cannot be explained by the conventional model for the HIFP [11] and may be one of characteristics of the HISR. One can speculate that the HISR brings about the shear deformation of the local glass structures resulting in a decrease in the elastic anisotropy around hydrogen atoms.

Figures 7(a) and 7(b) are redrawings of the ΔT_p *vs.* τ_H data shown in Fig. 3 but here ΔT_p and τ_H are plotted against the mean heat of solution, ΔH, estimated from the chemical composition of specimens and the heat of solution for elementary materials [21-23]. Except for *a*-$Zr_{50}Ni_{50}$, specimens can be classified into two groups, the low-ΔH group with $\Delta H < -10$ kJ/mol and the high-ΔH group with $\Delta H > -6$ kJ/mol. For the low-ΔH group, ΔT_p remains constant and τ_H shows an increase with increasing ΔH. For the high-ΔH group, both ΔT_p and τ_H shows an increase with increasing ΔH. The underlying mechanism for the ΔH dependence of ΔT_p and τ_H is not known at present, however, the present work demonstrates the new aspect for the HISR.

5. Conclusion

The C_H dependence of T_p and $Q^{-1}{}_p$ of the HIFP in *a*-$Zr_{55}Cu_{30}Al_{10}Ni_5$, *a*-$Zr_{54}Cu_{30}Al_{10}Ni_5Si_1$ and *a*-$Zr_{40}Cu_{49}Al_{10}Si_1$ were measured. It is found that the T_p *vs.* C_H data and the $Q^{-1}{}_p$ *vs.* C_H data are well explained by the relationships of $T_p = \Delta T_p \exp(-C_H/\tau_H) + T_{p,0}$ and $Q^{-1}{}_p \propto \ln(C_H/\tau_H)$, respectively, not only for all the present metallic glasses but also for various Zr-base metallic glasses reported. The characteristic C_H dependence of T_p and $Q^{-1}{}_p$ was attributed to effects of the hydrogen induced structural relaxation (HISR). The detailed features of the C_H dependence of T_p and $Q^{-1}{}_p$ were discussed in the light of material parameters and HISR.

Acknowledgement

This work is partly supported by a Grant in Aid for Scientific Research and the 21st Century Center of Excellence Program from the Ministry of Education, Culture, Sports, Science and Technology, Japan.

References

[1] H. Mizubayashi, S. Murayama, H. Tanimoto, J. Alloys and Compd. 330-332 (2002) 389.
[2] H. Mizubayashi, Y. Ishikawa, H. Tanimoto, Mater. Trans. 43 (2002) 2662.
[3] H. Mizubayashi, Y. Ishikawa, H. Tanimoto, J. Alloys and Compd. 355 (2003) 31.
[4] M. Hasegawa, S. Yamamura, H. Kato, K. Amiya, N. Nishiyama, A. Inoue, J. Alloys and Compd. 355 (2004) 37.
[5] M. Hasegawa, K. Kotani, S. Yamaura, H. Kato, I. Kodama, A. Inoue, J. Alloys and Compd. 365 (2004) 221.
[6] M. Hasegawa, M. Takeuchi, H. Kato, S. Yamaura, A. Inoue, J. Alloys and Compd. 372 (2004) 116.
[7] M. Hasegawa, M. Takeuchi, H. Kato, A. Inoue, Acta Mater. 52 (2004) 1799.
[8] T. Yagi, T. Imai, R. Tamura, S. Takeuchi, Mater. Sci. Eng. A 370 (2004) 264.
[9] H. Mizubayashi, Y. Ishikawa, H. Tanimoto, Mater. Sci. Eng. A 370 (2004) 546.
[10] H.-R. Sinning, J. Alloys and Compd. 310 (2000) 224.
[11] B.S. Berry, W.C. Pritchet, in: G. Bambakidis and R.C. Bowman, Jr. (Eds.), Hydrogen in Disordered and Amorphous Solids, Plenum Press, New York, 1986, p. 215.
[12] J.H. Harris, W.A. Curtin, M.A. Tenhover, Phys. Rev. B 36 (1987) 5784.
[13] M. Matsumoto, H. Mizubayashi, S. Okuda, Acta Metall. Mater. 43 (1995) 1109.
[14] A. Inoue, A. Takeuchi, Mater. Sci. Eng. A 375-377 (2004) 16.
[15] H. Mizubayashi, H. Agari, S. Okuda, Phys. Stat. Sol (a) 122 (1990) 221.
[16] L.K. Varga, K. Tompa, A. Lovas, J.M. Joubert, A. Percheron-Guegan, Int. J. Hydrogen Energy 21 (1996) 927.
[17] H. Mizubayashi, M. Shibasaki, S. Murayama, Acta Mater.48 (2000) 279.
[18] A. Inoue, Acta Mater. 48 (2000) 279.
[19] H. Mizubayashi, S. Hoshina, S. Okuda, J. Non-Crystalline Solids 117/118 (1990) 203.
[20] H. Mizubayashi, M. Kaida, S. Otsuka, S. Okuda, Acta Mater. 42 (1994) 2099.
[21] T. Ichimiya, A. Furuichi, Int. J. Appl. Radiat. Isot. 19 (1968) 573.
[22] E. Fromm, G. Horz, Int. Metals Rev. 25 (1980) 269.
[23] H. Wenzl, Intern. Metals Rev. 27 (1982) 140.

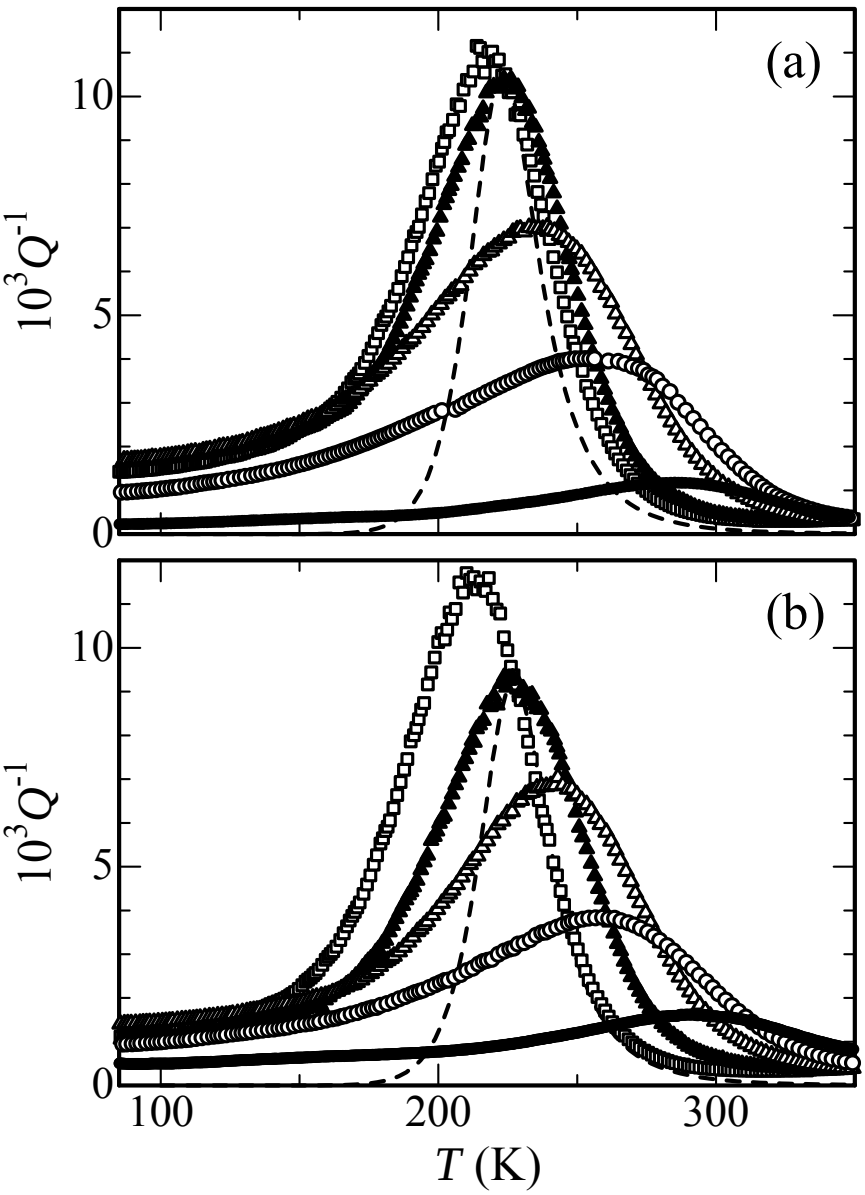

Fig. 1.
Examples of HIFPs observed at about 300 Hz : (a) *a*-$Zr_{55}Cu_{30}Al_{10}Ni_5$ (●: 1.1 at%, ○: 4.7 at%, △: 15.3 at%, ▲: 31.3 at%, □: 59.1 at%). (b) *a*-$Zr_{54}Cu_{30}Al_{10}Ni_5Si_1$ (●: 1.3 at%, ○: 5.1 at%, △: 15.8 at%, ▲: 30.4 at%, □: 64.4 at%). The dashed curves denote a theoretical Debye peak with $\tau_0 = 10^{-12}$ s and $E = 0.39$ eV.

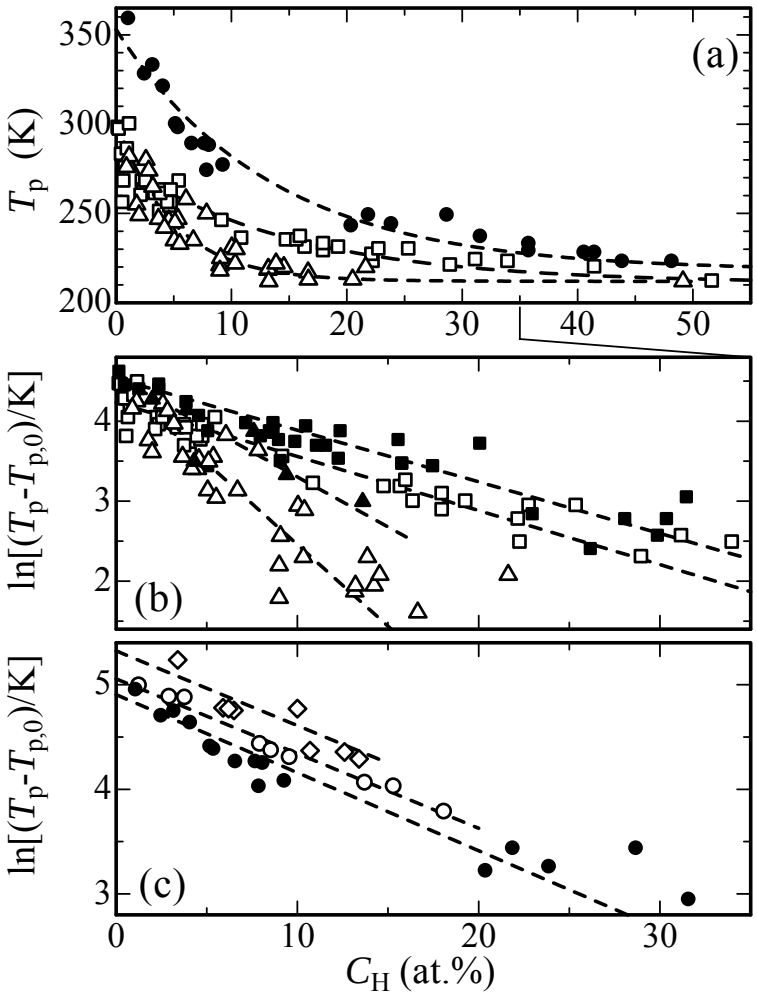

Fig. 2.
Examples of the T_p *vs.* C_H data ((a)) and examples of the $\ln(T_p-T_{p,0})$ *vs.* C_H data ((b), (c)) found for various a-alloys (●: *a*-$Zr_{40}Cu_{49}Al_{10}Si_1$ (after 400 K annealing), □: *a*-$Zr_{55}Cu_{30}Al_{10}Ni_5$, △: *a*-$Zr_{60}Cu_{30}Al_{10}$ [1], ■: *a*-$Zr_{54}Cu_{30}Al_{10}Ni_5Si_1$, ▲: *a*-$Zr_{59}Cu_{30}Al_{10}Si_1$ [2], ○: *a*-$Zr_{40}Cu_{50}Al_{10}$ [2], ◇: *a*-$Zr_{40}Cu_{49}Al_{10}Si_1$ (as-charged) [2]).

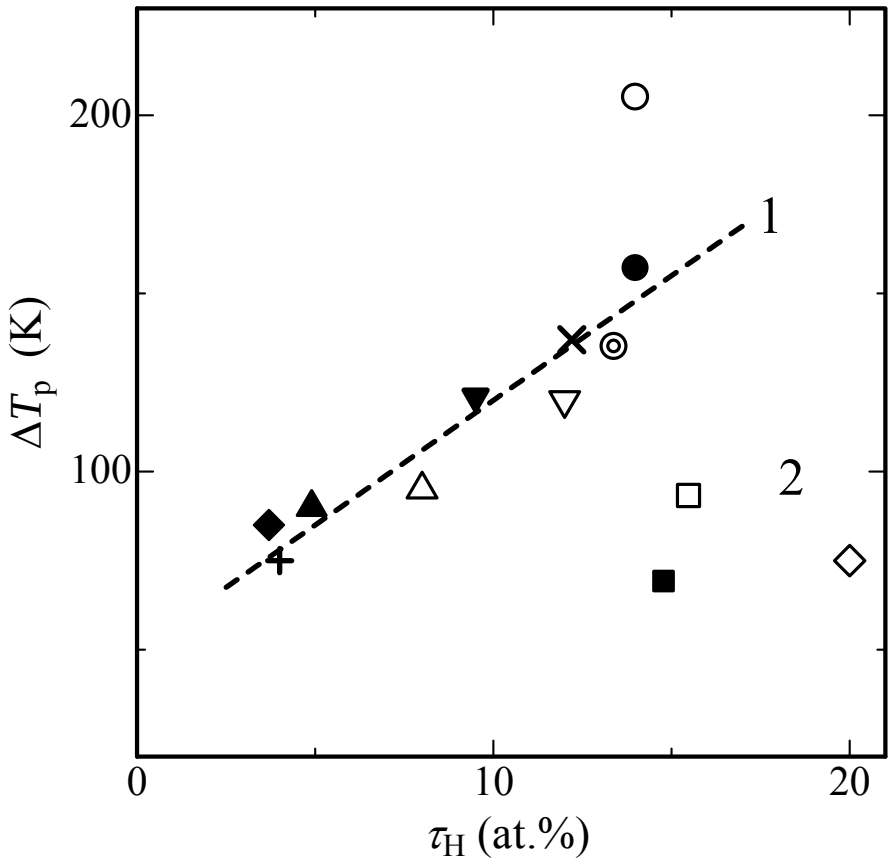

Fig. 3.
The ΔT_p *vs.* τ_H data observed for present specimens together with various metallic glasses reported. Group 1; ◆: *a*-$Zr_{60}Cu_{40}$ [1-3], ▲: *a*-$Zr_{60}Cu_{30}Al_{10}$ [1-3], △: *a*-$Zr_{59}Cu_{30}Al_{10}Si_1$ [1-3], ▽: *a*-$Zr_{40}Cu_{60}$ [13], ●: *a*-$Zr_{40}Cu_{50}Al_{10}$ [1-3], ○: *a*-$Zr_{40}Cu_{49}Al_{10}Si_1$ (as-charged) [1-3], ◎: *a*-$Zr_{40}Cu_{49}Al_{10}Si_1$ (after 400 K annealing), ▼: *a*-$Zr_{30}Cu_{60}Ti_{10}$, ×: *a*-$Zr_{50}Ni_{50}$, ＋: *a*-$Cu_{50}Ti_{50}$ [15]. Group 2; ■: *a*-$Zr_{55}Cu_{30}Al_{10}Ni_5$, □: *a*-$Zr_{54}Cu_{30}Al_{10}Ni_5Si_1$, ◇: *a*-$Zr_{50}Cu_{50}$ [1-3].

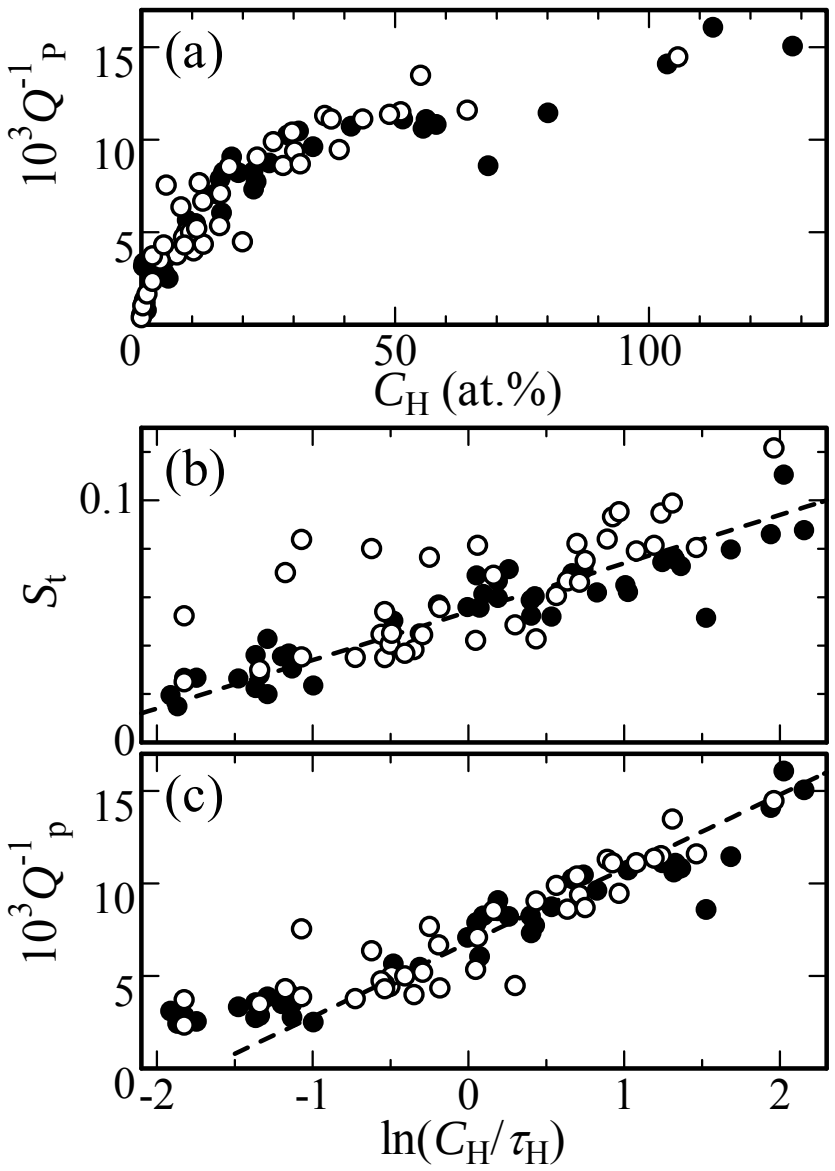

Fig. 4.
(a) The $Q^{-1}{}_p$ *vs.* C_H data, (b) the S_t *vs.* $\ln(C_H/\tau_H)$ data and (c) the $Q^{-1}{}_p$ *vs.* $\ln(C_H/\tau_H)$ data observed for *a*-$Zr_{55}Cu_{30}Al_{10}Ni_5$ (●, $\tau_H \approx 14.8$ at.%) and *a*-$Zr_{54}Cu_{30}Al_{10}Ni_5Si_1$ (○, $\tau_H \approx 15.5$ at.%). Dashed lines are drawn to guide eyes.

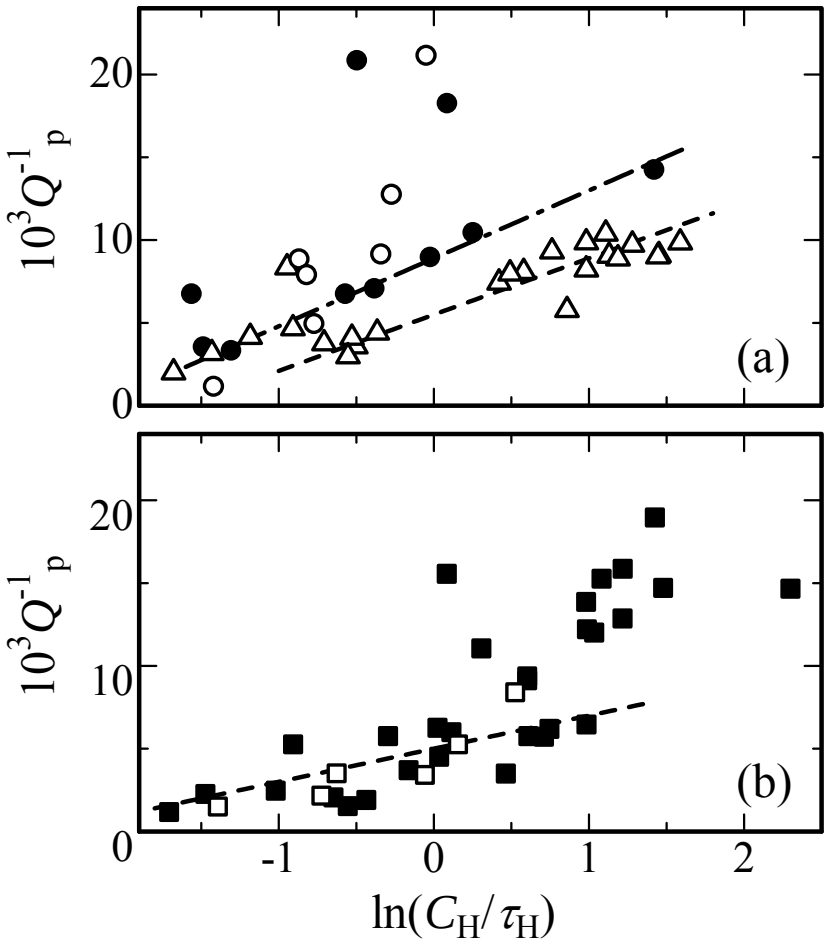

Fig. 5.
The S_t *vs*. $\ln(C_H/\tau_H)$ data observed for various metallic glasses: (a) : *a*-$Zr_{40}Cu_{50}Al_{10}$ (●, $\tau_H \approx 14$ at.%) ; *a*-$Zr_{40}Cu_{49}Al_{10}Si_1$ (as charged) (○, $\tau_H \approx 14$ at.%) ; *a*-$Zr_{40}Cu_{49}Al_{10}Si_1$ (after 400 K annealing) (△, $\tau_H \approx 13.4$ at.%). (b) : *a*-$Zr_{60}Cu_{30}Al_{10}$ (■, $\tau_H \approx 4.9$ at.%) ; *a*-$Zr_{59}Cu_{30}Al_{10}Si_1$ (□, $\tau_H \approx 8$ at.%). Dashed lines are drawn to guide eyes.

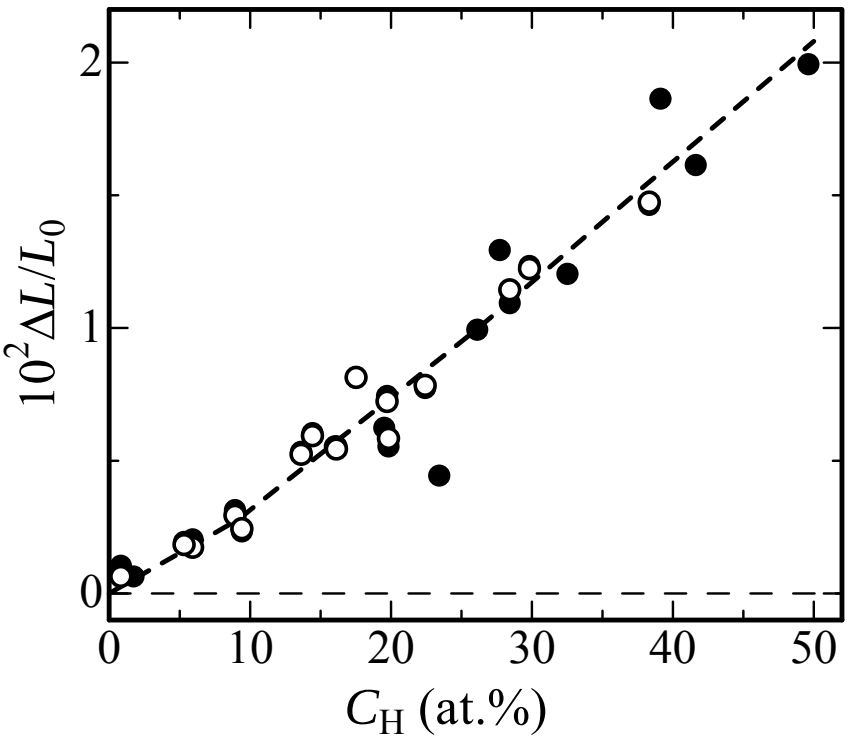

Fig. 6.
The $\Delta L/L_0$ *vs.* C_H data observed for *a*-$Zr_{40}Cu_{49}Al_{10}Si_1$ in the as charged state (●) and those after 400 K annealing (○). The dashed curve is tentatively fitted to the data points.

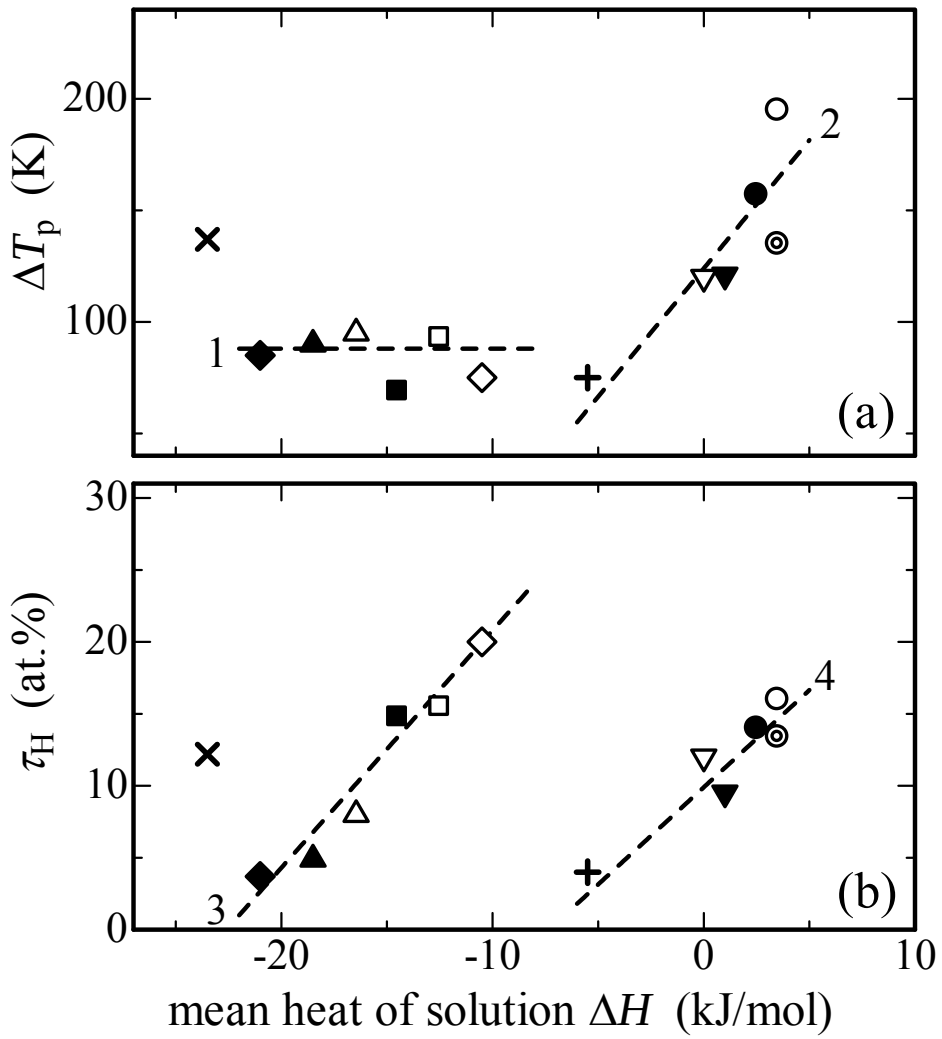

Fig. 7.
(a) The ΔT_p and (b) the τ_H data are plotted against the mean heat of solution. ◆: *a*-$Zr_{60}Cu_{40}$, ▲: *a*-$Zr_{60}Cu_{30}Al_{10}$, △: *a*-$Zr_{59}Cu_{30}Al_{10}Si_1$, ▽: *a*-$Zr_{40}Cu_{60}$, ●: *a*-$Zr_{40}Cu_{50}Al_{10}$, ○: *a*-$Zr_{40}Cu_{49}Al_{10}Si_1$ (as-charged), ◎: *a*-$Zr_{40}Cu_{49}Al_{10}Si_1$ (after 400 K annealing), ▼: *a*-$Zr_{30}Cu_{60}Ti_{10}$, ×: *a*-$Zr_{50}Ni_{50}$, ＋: *a*-$Cu_{50}Ti_{50}$, ■: *a*-$Zr_{55}Cu_{30}Al_{10}Ni_5$, □: *a*-$Zr_{54}Cu_{30}Al_{10}Ni_5Si_1$, ◇: *a*-$Zr_{50}Cu_{50}$. See text for details.